



Insights on ozone pollution control in urban areas by decoupling meteorological factors based on machine learning

5 Yuqing Qiu¹, Xin Li^{1,2*}, Wenxuan Chai^{3*}, Yi Liu¹, Mengdi Song¹, Xudong Tian⁴,
Qiaoli Zou⁴, Wenjun Lou⁵, Wangyao Zhang⁵, Juan Li⁵ and Yuanhang Zhang¹

¹College of Environmental Sciences and Engineering, Peking University, Beijing 100871, China

²Institute of Carbon Neutrality, Peking University, Beijing 100871, China

³China National Environmental Monitoring Center, Beijing 100012, China

⁴Zhejiang Ecological and Environmental Monitoring Center, Hangzhou 310012, China

10 ⁵Jinhua Ecological and Environmental Monitoring Center, Jinhua 321015, China

Correspondence to: Xin Li (li_xin@pku.edu.cn), Wenxuan Chai(chaiwx@cnemc.cn)

Abstract. Ozone (O₃) pollution is posing significant challenges to urban air quality improvement in China. The formation of surface O₃ is intricately linked to chemical reactions which are influenced by both meteorological conditions and local emissions of precursors (i.e., NO_x and VOCs). The atmospheric environment capacity decreases when meteorological conditions deteriorate, resulting in the accumulation of air pollutants. Although a series of emission reduction measures have been implemented in urban areas, the effectiveness of O₃ pollution control proves inadequate. Primarily due to adverse changes in meteorological conditions, the effects of emission reduction are masked. In this study, we integrated machine learning model, the observation-based model and the positive matrix factorization model based on four years of continuous observation data from a typical urban site. We found that transport and dispersion impact the distribution of O₃ concentration. During the warm season, positive contributions of dispersion and transport to O₃ concentration ranged from 12.9% to 24.0%. After meteorological normalization, the sensitivity of O₃ formation and the source apportionment of VOCs changed. The sensitivity of O₃ formation changed from the NO_x-limited regime to the transition regime between VOC- and NO_x-limited regimes during the O₃ pollution event. Vehicle exhaust became the primary source of VOC emissions after removing the effect of dispersion, contributing 41.8% to VOCs during the pollution periods. On the contrary, the contribution of combustion to VOCs decreased from 33.7% to 25.1%. Our results provided new recommendations and insights for implementing O₃ pollution control measures and evaluating the effectiveness of emission reduction in urban areas.

15
20
25
30



1 Introduction

Ozone (O_3) plays a significant role in atmospheric oxidation and global climate. It is also considered one of the major atmospheric pollutants. High concentration of surface O_3 is harmful to human health, such as causing respiratory diseases and even cancer (Cohen et al., 2017; Monks et al., 2015). In recent 35 years, China has been in a stage of rapid economic development, accompanied by the emergence of various air pollution problems due to industrialization and urbanization. (Zhang et al., 2012). In order to deal with the air pollution, the Chinese government has issued some control policies, such as Clean Air Action Plan in 2013 (Chinese State Council, 2013) and Blue-Sky Protection Campaign in 2018 (Chinese State Council, 2018). These policies have resulted in reductions in the concentrations of 40 particulate matter (PM), nitrogen dioxide (NO_2) and sulfur dioxide (SO_2) (Zheng et al., 2018). On the contrary, O_3 pollution has become increasingly serious, especially in the typical urban clusters such as the Beijing-Tianjin-Hebei (BTH), the Yangtze River Delta (YRD) and the Fenwei Plain (FWP). In 2022, the 90th percentile of maximum daily 8 h average (MDA8) O_3 were $179 \mu\text{g}/\text{m}^3$ in the BTH, $162 \mu\text{g}/\text{m}^3$ in the YRD and $167 \mu\text{g}/\text{m}^3$ in the FWP, 4.7%, 7.3% and 1.2% higher than that in 2021, 45 respectively (Ministry of Ecology and Environment of China, <https://www.mee.gov.cn/>). Frequent O_3 pollution events have attracted the attention of the public and the government. Surface O_3 is mainly formed by the photochemical reactions of volatile organic compounds (VOCs) and nitrogen oxides ($NO_x = NO + NO_2$) (Atkinson, 2000). The emissions of precursors effectively affect the change of O_3 concentration (Tan et al., 2018). The sources of VOCs are complex and widespread, making it 50 challenging to control emissions. Meteorological conditions can directly or indirectly affect O_3 concentration (Liu and Wang, 2020; Zhang et al., 2015). Wind and boundary layer height influence the diffusion of the concentrations of O_3 and its precursor. Poor dispersion can result in a decrease in atmospheric environmental capacity, making O_3 pollution events more likely to occur even with low precursor emissions. High ultraviolet radiation and temperature promote photochemical reactions of O_3 55 formation (Yang et al., 2019). In addition, O_3 can be transported over long distances due to its the long atmospheric lifetime, which can cause regional O_3 problems (Han et al., 2019). In short, the O_3 concentration is nonlinear affected by meteorological conditions, emissions of precursors and chemical reactions (Fu et al., 2019; Hu et al., 2021).



Li et al. (2020) discovered that approximately 1/3 of the growth of O₃ concentration in summer in
60 China was attributed to meteorological conditions. This indicated that the reduction of air pollutants
concentrations due to the control policies may be offset by the deterioration of meteorological
conditions. Therefore, decoupling meteorological factors from temporal concentrations series of
atmospheric pollutants is helpful to assess the impact of clean air action. At present, many
mathematical statistical methods have been developed to remove the influences of meteorological
65 factors. The technique for predicting air pollutants concentrations under randomly selected
meteorological parameters was first introduced by Grange et al. (2018). Weng et al. (2022) found that
the temperature near the surface 2 m, the downward radiation flux of the surface and the relative
humidity were the most important meteorological factors to affect O₃ concentration in China by
applying two machine learning algorithms (ridge regression and random forest regression).
70 Mousavinezhad et al. (2021) employed the Kolmogorov-Zurbenko (KZ) filter method and found that
meteorological factors played the dominant role on O₃ formation in four typical urban agglomerations
in China. Guo et al. (2022) used the random forest method to obtain the characteristics of air pollution
in 12 megacities in China from 2013 to 2020, and carried out a comprehensive assessment of the actual
impact of the national clean air action. Compared to traditional statistical methods, machine learning
75 models perform better in removing meteorological effects from concentration data.

In response to severe O₃ pollution, a series of emission reduction measures targeting O₃ precursors have
been implemented in urban areas. However, the effectiveness of controlling O₃ pollution fell short of
expectations. According to previous studies, O₃ formation in urban areas was more sensitive to VOCs
(Feng et al., 2019), with anthropogenic emissions of VOCs playing a dominant role (Ahmad et al.,
80 2017). Understanding the sensitivity of O₃ formation and the source characteristics of VOCs are
helpful to design effective strategies to control O₃ pollution. The basis for precursor emission reduction
policies relies on the observation-based model (OBM) or the positive matrix factorization model
(PMF), but the model results based on observed data are influenced by fluctuations of meteorological
conditions. Wu et al. (2023) developed initial concentration dispersion normalized PMF (ICDN-PMF)
85 to reflect changes in source emissions of VOCs in Qingdao. The results proved that the contribution of
solvent use overestimated due to air dispersion during O₃ pollution. Additionally, the actual
effectiveness of emission reduction measures can also be obscured by unfavorable meteorological
conditions. In this study, we applied the Random Forest (RF) method proposed by Grange et al. (2018)



to remove the dispersion and transport effects on O₃ concentration, as well as the dispersion effect on
90 precursors in Hangzhou from 2019 to 2022. After meteorological normalization, the concentrations of
VOCs were imported into OBM and PMF to obtain the sensitivity of O₃ formation and the
contributions of emission sources, providing more accurate results. The interplay of meteorological and
local factors on O₃ pollution can be evaluated effectively and comprehensively in this method. Our
results emphasized the importance of decoupling the meteorological effects of transport and dispersion
95 for understanding the mechanisms of local O₃ formation and devising appropriate emission reduction
measures.

2 Methods

2.1 Observation data

The online hourly observation data from 2019 to 2022 were measured by the Zhejiang Ecological and
100 Environmental Monitoring Center (30.29°N, 120.13°E). This station was located in the urban area of
Hangzhou, Zhejiang Province, surrounded by residential and commercial areas. The data set of air
pollutants included O₃, NO₂ and 98 different kinds of VOCs detected by gas chromatography system,
including 29 alkanes, 11 alkenes, 1 alkyne, 16 aromatics, 28 halohydrocarbons, 12 oxygenated VOCs
(OVOCs), and 1 acetonitrile. The online gas chromatography system was equipped with a mass
105 spectrometer and flame ionization detector (GC-MS/FID), which used a dual gas path separation
method. VOCs compounds with low carbon numbers (C₂-C₅) were measured by FID, while VOCs
compounds with high carbon numbers (C₅-C₁₀) were detected by MS. Meteorological parameter
contained temperature (T), relative humidity (RH), atmospheric pressure (P), wind speed (WS) and
wind direction (WD). In addition, we used the meteorological data from the ERA5 reanalysis product
110 (Hersbach et al., 2020), such as boundary layer height (BLH) and ultraviolet radiation b (UVB). The
EAR5 meteorological data is spatial grid data with a resolution of 0.25°×0.25° and available at
<https://cds.climate.copernicus.eu/cdsapp>. The back trajectories were calculated backwards in time for
24 h and started 500 m above ground level by using the Hybrid Single Particle Lagrangian Integrated
Trajectory (HYSPPLIT) model (Stein et al., 2015). The meteorological data from the Global Data
115 Assimilation System (GDAS) with a horizontal resolution of 1° longitude × 1° latitude were adopted in



trajectory model. The back trajectories were then clustered into five clusters by using the Euclidian distance.

2.2 Meteorological normalization method

Random Forest is a versatile classifier that comprises multiple decision trees, applicable to classification, regression, and dimension reduction problems. When constructing each tree in the RF model, a dataset of the same size is selected for training, potentially containing duplicates. This sampling method, which involves putting instances back into the dataset, is referred to as bootstrap. At each node, the optimal segmentation is calculated by randomly selecting a subset of features from the entire set. The RF model describe the relationship between the time series of atmospheric pollutants concentrations and their corresponding feature. We constructed random forest model based on original datasets, which contained air pollutants variables (O₃, NO₂, total non-methane hydrocarbon compounds (NMHCs) and 98 VOC species), time variables (trend, hour, weekday, month and day of year) and meteorological variables (T, RH, P, WS, WD, UVB, BLH and cluster). T, RH and UVB can characterize the local production and loss by chemical reactions. WD, WS and BLH are crucial for the dispersion of O₃ and its precursors on a local scale. While cluster can reflect the effect of transport from remote regions. The parameter ‘trend’ can indicate the long-term changes of air pollutants concentrations resulting from the implementation of policy measures (Vu et al., 2019), which was calculated as Eq. (1):

$$\text{trend} = \text{year}_i + \frac{t_{\text{D}} - 1}{N_i} + \frac{t_{\text{H}}}{24N_i} \quad (1)$$

Where N_i is the number of days in the year_i (year_i is from 2019 to 2022), t_H is hour time (0~23), t_D is day of the year (1~365) (Carslaw and Taylor, 2009).

Training datasets of the RF model was conducted on 80% of the original datasets, and the remaining 20% was selected as testing datasets. In the meteorological normalization process of O₃ concentration, meteorological variables such as WS, WD, BLH, and cluster, which signify dispersion and transport, were randomly sampled. In the case of O₃ precursors, namely NO₂ and NMHCs, resampling was exclusively applied to WS, WD and BLH. NO₂ and NMHCs have short atmospheric lifetimes, making them less susceptible to the influence of regional transport over large scales (Wang et al., 2023). The resampled specific meteorological variables, along with other initial variables, were fed into the RF



model to predict air pollutants concentrations. The resampling and prediction process were repeated
145 1000 times to generate 1000 predicted pollutants concentrations. The average values were taken as the
final meteorological normalized concentrations. The RF model was constructed using R “deweather”
packages developed by Carslaw (<https://github.com/davidcarslaw/deweather>).

2.3 Observation-based model

An observation-based model is used in this study to simulate the formation of O₃. The model is based
150 on Regional Atmospheric Chemical Mechanisms version 2 (RACM2) updated with detailed isoprene
oxidation mechanism (Goliff et al., 2013). As a 0-D model, this model incorporates dilution mixing
within the boundary layer. However, vertical or horizontal transport of the air mass is not considered in
this model. Detail of the observation-based box model can be found in Tan et al. (2017). The photolysis
frequencies (J values) were calculated by using the Tropospheric Ultraviolet and Visible (TUV) model
155 (Wolfe et al., 2016). Model calculations were constrained to measured trace gases, including inorganic
species (NO₂ and O₃) and organic species (VOCs). Besides, physical parameters like J values,
temperature, pressure and relative humidity were also constrained to measured values. The empirical
kinetic modeling approach (EKMA) serves as a sensitivity test for the OBM. EKMA curve offers a
means to quantify intricate nonlinear relationships among O₃, NO_x and VOCs, which can be used as a
160 theoretical basis for designing O₃ pollution reduction strategies (Tan et al., 2018). In this study, a total
of 30 emission scenarios were established for both NO_x and anthropogenic VOCs. Subsequently, O₃
concentrations resulting from changes in these precursor emissions were simulated across 900
scenarios. The EKMA curve was plotted according to the O₃ formation rate under different VOCs and
NO_x conditions.

2.4 Positive matrix factorization

The positive matrix factorization model is based on a large number of data to estimate the compositions
and contributions of emission sources (Paatero and Tapper, 1994). The PMF model is widely used for
VOCs source apportionment (Song et al., 2021; Yuan et al., 2010). In the PMF model, it is assumed
that the pollutants concentrations measured at the receptor point can be represented as a linear sum of
170 components emitted by different sources. Indeed, the temporal variation of atmospheric pollutants is
influenced not only by emissions but also by dispersion. Direct PMF analysis based on observed data



may lead to the loss of real information regarding emission sources. In this study, the observed and meteorological normalized VOCs concentrations were fed into US EPA PMF v5.0 to identify and quantify major emission sources of VOCs. In contrast to the PMF results based on observation, examining the alterations in contributions of emission sources after meteorological normalization can reveal the impact of dispersion on VOCs sources.

3 Results and discussion

3.1 Temporal variations of O₃ and its precursors

3.1.1 Long-term variations

The RF model demonstrated effective performance in predicting most of the air pollutants. The R² values of O₃, NO₂ and NMHCs were 0.88, 0.83 and 0.76, respectively. The R² values of 81% VOC species were in the range of 0.5 to 0.96, and the R² values of a few VOC species with low concentrations were lower than 0.4. Fig. 1 displayed the time series of air pollutants concentrations based on observation and meteorological normalization from 2019 to 2022. After meteorological normalization, the concentrations of O₃ and its precursors were primarily affected by local factors, including precursors emission and chemical reactions. From a long-term perspective, the trends of air pollutants concentrations after meteorological normalization were consistent with those based on observation. This indicated that the variation in O₃ concentration in Hangzhou was mainly driven by precursors emissions and chemical formation in the long term.

From the diurnal trends of NO₂ and NMHCs, the observed concentrations were lower during the day and higher at night, which was contrary to the daily trends of WS and BLH (Fig. S1). Stable WS and low BLH at night were not conducive to the diffusion of air pollutants, resulting in the accumulation of pollutants concentrations, while the situation was opposite during the day (Song et al., 2018). After the dispersion effect was removed, the precursors concentrations decreased at night and increased significantly during the day. The diurnal variation of O₃ concentration showed a typical single-peak structure before and after meteorological normalization. Different from the change in the concentrations of precursors, the O₃ concentration increased at night and decreased during the day after meteorological normalization. At night, the titration reaction of NO_x and the horizontal transport reduced the O₃ concentration (Li et al., 2022). The NO_x concentration decreased after meteorological



200 normalization, and the weakening of titration resulted in the increase of O₃ concentration at night. In addition, the decrease in horizontal transport at night also resulted in the increase of O₃ concentration after normalization. During the day, the destruction of the stable boundary layer strengthened the vertical mixing effect of the atmosphere, so that the O₃ in the upper atmosphere mixed with the O₃ generated near the surface, increasing the O₃ concentration (Lei et al., 2023). When the effect of

205 transport was removed, the daytime O₃ concentration decreased. It can be seen from the diurnal variations that meteorological factors directly affected the concentrations of precursors through dispersion. And meteorological factors not only directly affected the O₃ concentration through horizontal and vertical transport, but also indirectly change O₃ concentration by influencing precursor concentration and titration reaction.

210

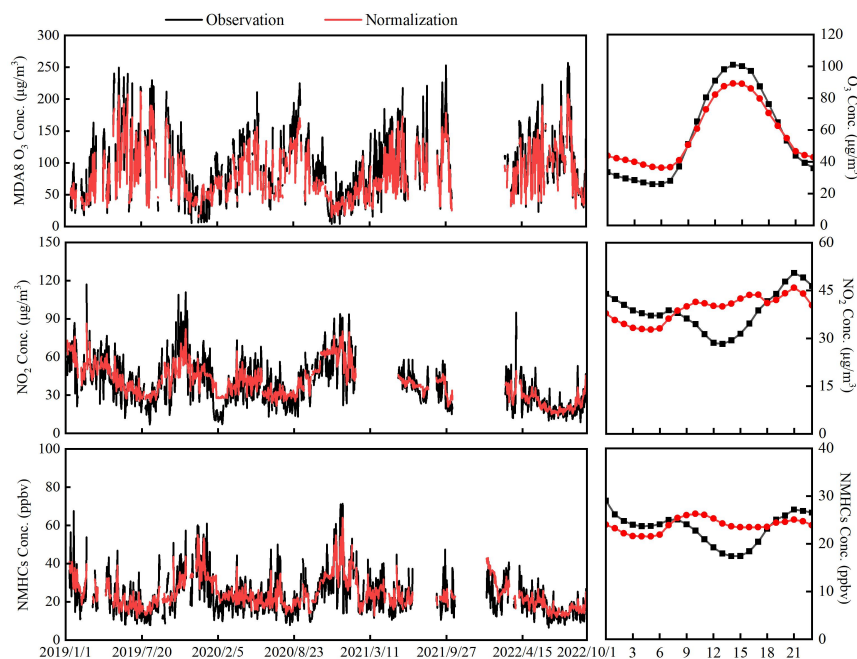


Figure 1: Long-term trends of daily average concentrations of air pollutants (left) and mean diurnal variations of air pollutants concentrations (right) based on observation and meteorological normalization from 2019 to 2022.

215

Fig. 2 showed the importance of the different features in the RF model. The time variables can represent anthropogenic emissions to some extent. The chemical reaction of O₃ formation was affected



by meteorological factors such as UVB, T and RH. Local dispersion of O₃ and its precursors was mainly affected by WS, WD and BLH, and long-distance transport of O₃ was characterized by cluster.

220 The importance of local chemical reactions to O₃ was 83.9%. UVB, influencing photochemical reactions, emerged as the most crucial factor for O₃ concentration, with an importance of 25.9%. This is consistent with the findings by WENG et al. (2022) in the same region. Additionally, the importance of RH and T to O₃ was also evident, with the importance of 18.2% and 11.3% respectively. Relative humidity was related to cloud cover, exerting an indirect influence on aerosol radiation (Gao et al.,

225 2021; Ma et al., 2021). Further considering the complex HO_x chemical reactions, humidity and O₃ concentration were usually negatively correlated (Han et al., 2020). High humidity can enhance the reaction of O(¹D) produced by O₃ photolysis and H₂O: O(¹D) + H₂O → 2OH (Wang et al., 2013). The influence of temperature on O₃ formation stemmed from the fact that the chemical kinetic rate increased with rising temperature (Li et al., 2020). Besides, elevated temperature enhanced the

230 emission of biogenic VOCs (Lu et al., 2019). Hence, some O₃ pollution events were associated with high temperature (Dang et al., 2021). Ding et al. (2023) found that temperature was the dominant factor affecting O₃ concentration in Tianjin. Wind and BLH also played significant roles in O₃ concentration (16.1%), mainly through vertical diffusion, vertical convection and horizontal convection (Li et al., 2012).

235 Different from O₃, BLH exerted a most significant impact on NO₂ and NMHCs variation, with the importance value of 26.1% and 20%, respectively. Turbulent mixing in the active boundary layer facilitated the dispersion of air pollutants, whereas the stable boundary layer attenuated vertical diffusion, thereby intensifying the accumulation of air pollutants near the ground. (Huang et al., 2020). The importance of dispersion to NO₂ and NMHCs was 34.2% and 30.7, respectively. Consequently,

240 unfavorable meteorological dispersion conditions can result in the accumulation of precursors, causing O₃ pollution even in scenarios with low emissions. Temporal variables representing emissions, such as month and day of year, also occupied important positions. The importance of month to NO₂ and NMHCs exceeded 18%, which represented the significant influences of seasonal anthropogenic emissions on the concentrations of precursors. The importance of local emission, production and

245 consumption to NO₂ and NMHCs were 65.8% and 69.3%, respective (Fig. 2).

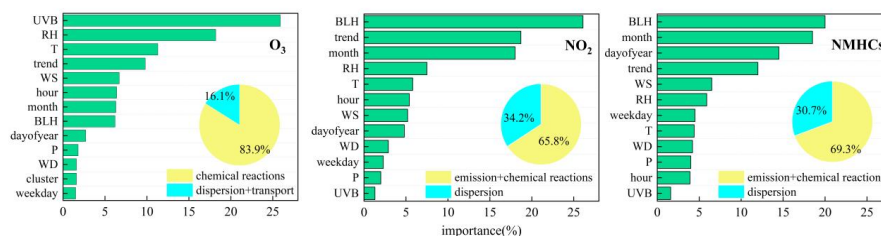
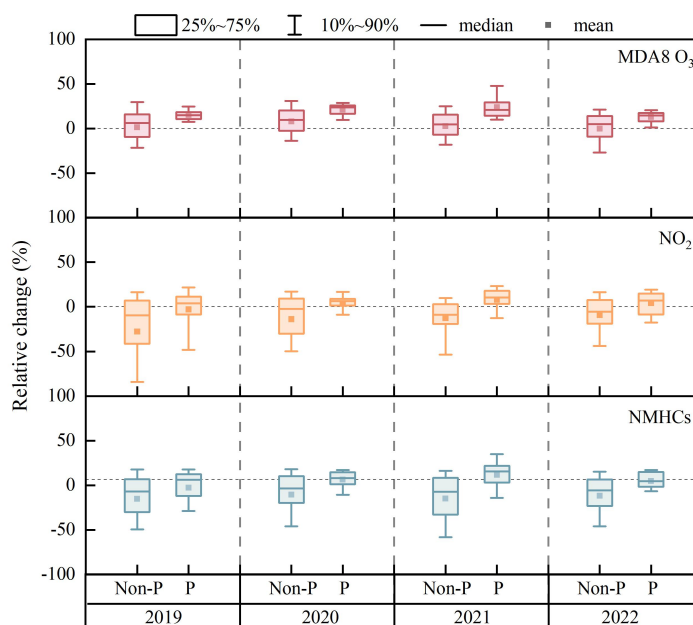


Figure 2: The importance of each feature to O₃, NO₂ and NMHCs in the RF model.

250 3.1.2 Comparison between pollution and non-pollution periods

O₃ pollution occur frequently between May and September each year. In order to evaluate the influences of meteorological conditions on the concentrations of O₃ and its precursors, the relative change of air pollutants concentrations caused by meteorological factors during O₃ pollution and non-pollution periods in warm season from 2019 to 2022 was analyzed. In the non-pollution periods, the negative effect of dispersion on the concentrations of NO₂ and NMHCs was apparent, with average relative changes ranging from -9.3% to -27.98% for NO₂ and -10.5% to -22.8% for NMHCs. Dispersion and transport have less influences on the MDA8 O₃ concentrations, with average relative change ranging from -0.1% to 8.1%. During the pollution periods, the positive effects of dispersion and transport on O₃ became evident (from 12.9% to 24.0%). Simultaneously, the negative effect of dispersion on the concentrations of precursors decreased and even transformed into positive effect. Especially in 2021, dispersion had a significant positive effect on NO₂ and NMHCs, with an average relative change of 7.8% and 11.8%, respectively. O₃ concentration was affected by the long-distance transport as well as the deterioration of diffusion conditions in the pollution periods. Therefore, the influences of meteorological factors on O₃ was more obvious than that of its precursors during pollution periods in the warm season.



270 **Figure 3: Relative change caused by meteorological factors during O₃ pollution (P) and non-pollution (Non-P) periods in the warm season from 2019 to 2022, relative change = the observed concentrations - the meteorological normalized concentrations/the observed concentrations.**

3.1.3 Variations during short-term pollution events

In order to explore the effects of meteorological dispersion and transport on O₃ concentration in the short term, we selected two typical pollution periods from 2019 to 2022. During the Period 1 (August 31 to September 13 in 2020), the average MDA8 O₃ in Hangzhou was 193 μg/m³ in the pollution, exceeding the national air quality standard (> 160 μg/m³, GB 3095-2012). At the same time, other cities in the YRD regions such as Shanghai, Nanjing, Wuxi, Changzhou, Suzhou and Jiaxing also experienced O₃ pollution (Fig. S2). The Period 1 represented a large-scale regional pollution event. During the pre-pollution (August 31 to September 2 in 2020), dispersion and transport had negative effects on MDA8 O₃. In the pollution periods (September 3 to September 10 in 2020), the concentration of locally generated O₃ (depicted by the red line) remained below the limit, with an average concentration of 157 μg/m³, with only slight exceedances recorded on September 6 and September 9. However, the actual observed O₃ concentration was much higher than the standard, and the O₃ concentration was about 200 μg/m³ from September 6 to September 10. The positive

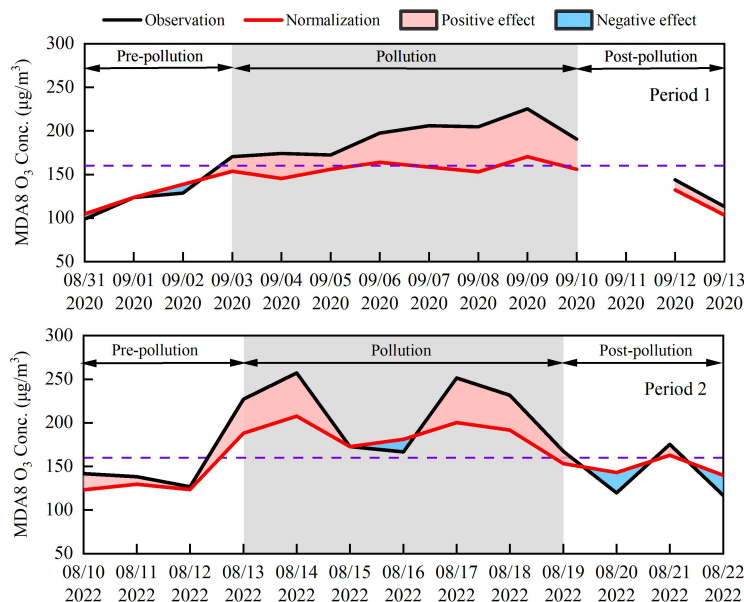
275

280



285 contributions of dispersion and transport was significant (depicted by the red area) in the pollution periods, resulting in an 18.7% increase in the MDA8 O₃ concentration. During the post-pollution period, contributions of dispersion and transport decreased significantly.

In the Period 2 (August 10 to August 22 in 2022), the average MDA8 O₃ concentration in Hangzhou was as high as 211 µg/m³ during the pollution, while the concentration of MDA8 O₃ in most surrounding cities was less than 160 µg/m³. Thus the O₃ pollution in the Period 2 was influenced by both local formation and transport. During the pollution periods (August 13 to August 19 in 2022), locally generated O₃ basically exceeded the standard, and the MDA8 O₃ concentration was greater than 180 µg/m³ on most days, with an average concentration of 185 µg/m³. On August 16, the meteorological negative contribution (-14.4%) appeared, exerting dilution effects on the O₃ concentration, but the MDA8 O₃ on that day still exceeded 160 µg/m³, indicating intense local O₃ production. The positive contributions of dispersion and transport to O₃ were significant during the pollution periods, the contributions ranged from 8.5% to 20.4%. For precursors, the concentration of NMHCs increased between 17 and 19 August (Fig. S3). The positive contribution of dispersion to NO₂ and NMHCs ranged from 4.4% to 13.7% and from 0.6% to 8.5% in pollution. During the post-pollution (August 20 to August 22 in 2022), the contributions of dispersion and transport turned negative, indicating that meteorological diffusion conditions were in favor to the elimination of O₃ pollution.



305 **Figure 4: The MDA8 O₃ concentration based on observation and meteorological normalization, and the contributions of dispersion and transport to the MDA8 O₃ during pre-pollution, pollution and post-pollution in the Period 1 and Period 2 (red: positive contribution, blue: negative contribution).**

3.2 VOC-NO_x-O₃ sensitivity

310 Unfavorable meteorological conditions can cause the accumulation of O₃, making it essential to have a clear understanding of local O₃ formation pathways for effective control of O₃ pollution. The relationship between O₃ and NO₂ under long-term trends was analyzed based on the observed and meteorological normalized data (Fig. 5). The red dotted line showed the turning point of the relationship between O₃ and NO₂ concentrations. On the left side of the red dotted line, O₃ concentration elevated with the increase of NO₂ concentration. At this point, controlling the emission of NO₂ was conducive to limiting the formation of O₃, suggesting that the sensitivity of O₃ formation was limited by NO_x. On the right side of the red dotted line, O₃ concentration decreased with the increase of NO₂ concentration. At this point, the inhibition effect of NO_x emission reduction on O₃ formation was not significant, and it is necessary to control the emission of VOCs, indicating that the sensitivity of O₃ formation was limited by VOCs (Kong et al., 2024). After meteorological normalization, the NO₂ concentration in the turning point increased from 9 µg/m³ to 19 µg/m³, suggesting when NO₂

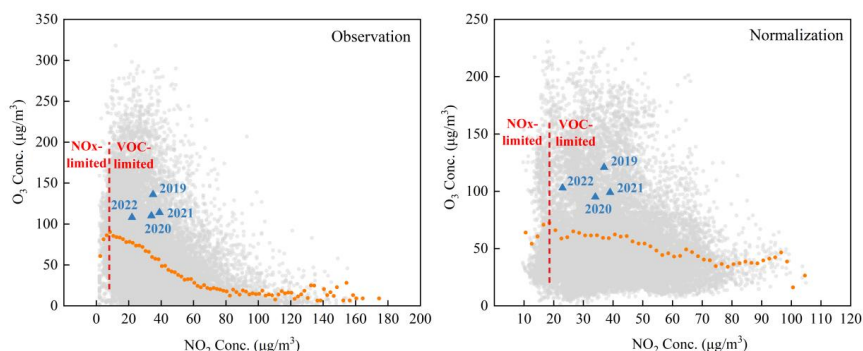
315

320



concentration was at a higher level, O₃ concentration decreased with the increase of NO₂ concentration. In other words, the actual O₃ production enter the VOC-limited regime more slowly. In addition, based on average results in warm season each year, the sensitivity of O₃ formation before and after meteorological normalization was also shown in Fig. 5. Whether based on observed or meteorological

325 meteorological normalization was also shown in Fig. 5. Whether based on observed or meteorological normalized data, the O₃ formation from 2019 to 2021 was located in the VOC-limited regime, while O₃ production enter the transition regime between VOC- and NO_x-limited regimes. in 2022.



330 **Figure 5: The changes of O₃ concentration on NO₂ concentration from 2019 to 2022. The light gray circles represented the hourly O₃ concentration. The orange circles represented the average value of O₃ concentration in each interval (2 µg/m³) of NO₂. The blue triangle represented the average value of the MDA8 O₃ during the warm season each year.**

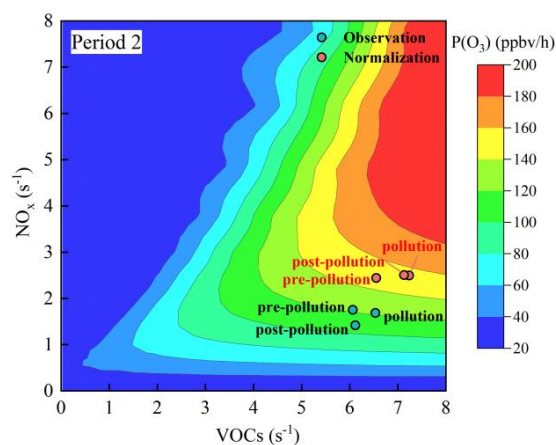
335 The OBM was used to analyze the sensitivity of O₃ formation. The OBM is zero-dimensional, meaning it excludes the processes of atmospheric transport and dispersion. Therefore, it is reasonable to remove the influences of transport and dispersion when using the OBM. The VOC-NO_x-O₃ sensitivity and the net ozone production rate (P(O₃)) exhibited significant differences before and after meteorological normalization in the short-term pollution events (Fig. 6). The O₃ concentration in the Period 2 was

340 affected by both transport and local formation. The concentration of local precursors increased after removing the effect of dispersion, resulting in the change of the sensitivity of O₃ formation. Based on the observation results, the O₃ formation in pollution was located in the NO_x-limited regime. After meteorological normalization, O₃ formation enter the transition regime between VOC- and NO_x-limited regimes. Besides, the meteorological normalized P(O₃) was improved after removing the effect

345 of transport on O₃ concentration. Therefore, when OBM was used to analyze the VOC-NO_x-O₃



sensitivity, removing the influences of dispersion and transport was beneficial to accurately identify the limited regime of O₃ formation.



350 **Figure 6: The O₃ isopleth diagram versus NO_x and anthropogenic VOCs by using EKMA. The circles represented the average concentrations of NO_x and VOC during pre-pollution, pollution and post-pollution in the Period 2.**

3.3 VOCs source apportionment

355 The PMF method was further used for VOCs source analysis. The optimal solution was selected by examining the interpretability of factors and the distribution of scale residuals. Based on observed and meteorological normalized concentrations, seven possible emission sources of VOC from May to September in 2022 were extracted by using the US EPA PMF v5.0. The possible emission sources of VOC included combustion, industrial source, vehicle exhaust, fuel evaporation, secondary and aging
 360 source, biogenic source and solvent use. The differences in the source profiles resolved from the observed and normalized concentrations were illustrated in Fig. S4.

Combustion source was characterized by high concentrations of ethane, propane, and acetylene. Low carbon alkanes and alkenes were likely to be the products of incomplete combustion (Wang et al., 2015). Acetylene was a typical tracer of combustion. Toluene and some halohydrocarbons, such as
 365 chloromethane, were also released from combustion (Liu et al., 2008). Additionally, the proportion of acetonitrile was also high, which was an important product of biomass combustion (De Gouw et al., 2003). Biomass combustion emission was relatively intense in the YRD. Industrial source was



characterized by halohydrocarbons (Sun et al., 2016), and 1,2-dichloroethane accounted for nearly 80% of this factor in both PMF results. Vehicle exhaust was featured by high concentrations of ethane, propane, isobutane, n-butane, isopentane, ethylene and toluene (Cai et al., 2010; Liu et al., 2008). Fuel evaporation was characterized by the high concentration and proportion of isopentane, isobutane, n-butane and n-pentane. While the concentration of acetylene was minimal in this factor. Secondary and aging source was characterized by halohydrocarbons and oxygenated VOCs (OVOCs). Methacrolein (MACR) and methyl vinyl ketone (MVK) were products of the oxidation of isoprene (Mo et al., 2018). OVOC and halohydrocarbons have long lifetimes in the atmosphere and can serve as important tracers for aging sources (Yang et al., 2021). Biogenic source was featured by highest concentration of isoprene, primarily emitted by plants (Gong et al., 2018). Additionally, the oxidation products of isoprene (MACR and MVK) also contributed to this factor. Solvent source was characterized by high concentrations of aromatics. Toluene, ethylbenzene, m-xylene and o-xylene, which were commonly used as the materials in solvents (Song et al., 2021).

After normalizing the effect of dispersion, the absolute contribution of emission sources to VOCs changed. The mean absolute contribution of vehicle exhaust to VOCs increased most significantly, from 3.97 ppbv to 6.72 ppbv during the non-pollution periods, and from 6.84 ppbv to 9.76 ppbv during the pollution periods. The mean absolute contribution of combustion decreased by 1.55 ppbv and 2.09 ppbv to 2.86 ppbv and 5.85 ppbv during the non-pollution and pollution, respectively. Dispersion caused overestimation of the contribution of combustion to VOCs, which indicated the reduction in VOCs concentration by abatement measures can be offset by the effect of dispersion. Therefore, the impact of dispersion should be taken into account when evaluating the effectiveness of emission reduction measures on VOCs emission sources. The normalized contributions of solvent use and industrial source in the pollution were comparable, with an average absolute contribution of 2.78 ppbv and 2.57 ppbv. In comparison to the result based on observation, the absolute contribution of fuel evaporation decreased from 1.94 ppbv to 1.33 ppbv after meteorological normalization during the pollution periods. After meteorological normalization, the contributions of biogenic source and secondary and aging source to VOCs during the pollution period were relatively low, with absolute contributions of 0.54 ppbv.

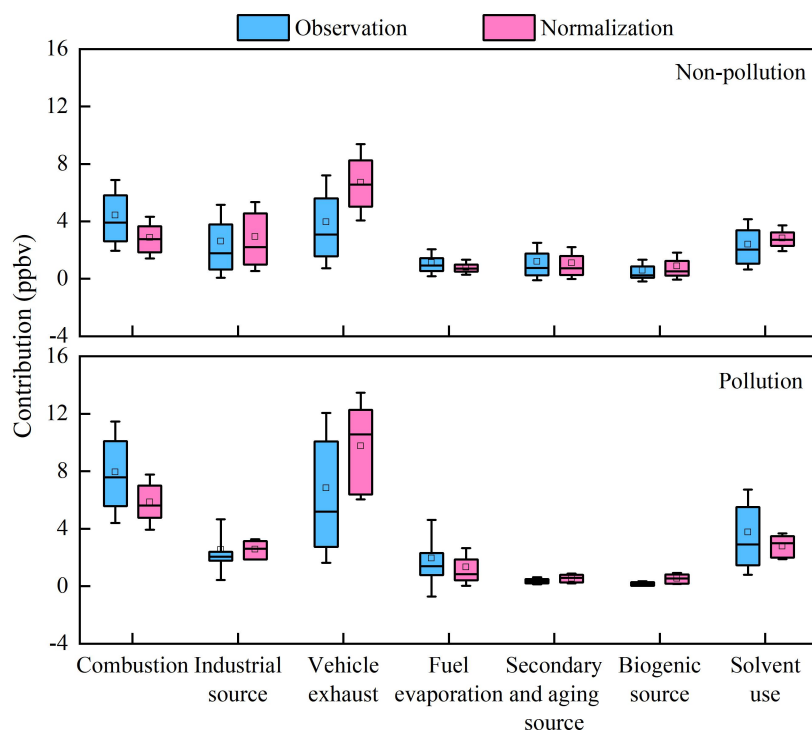


Figure 7: The absolute contributions of emission sources to VOCs based on observation and meteorological normalization during the non-pollution periods and pollution periods in the warm season in 2022.

400

Fig. 8 showed the proportion of VOCs sources before and after meteorological normalization during the non-pollution periods and pollution periods. According to the result of observation, combustion and vehicle exhaust were the largest contributors to VOCs, accounting for 27.1% and 24.3% in the non-pollution periods. And the proportion of combustion and vehicle exhaust increased to 33.7% and 29% in the pollution periods. During the pollution periods, the proportion of solvent use and fuel evaporation also increased, accounting for 15.9% and 8.2%, respectively. After the normalization of dispersion, vehicle exhaust became the predominant emission source of VOCs (37% in the non-pollution periods and 41.8% in the pollution periods), much higher than the proportion of other emission sources. According to the motor vehicle data released by the Zhejiang Public Security Department in 2022, the number of motor vehicles reached 23.29 million. During the non-pollution periods, the contributions of solvent use, industrial source and combustion were comparable, accounting for the proportions ranging of 15.6% to 16.2%. However, the influence of combustion on

405

410



VOCs increased (25.1%), while the proportion of industrial source and solvent use decreased during the pollution periods (11% and 11.9%). Straw burning occurred frequently in Zhejiang Province. According to the remote sensing monitoring of straw burning announced by the Ecological Environment Monitoring Center of Zhejiang Province, a total of 135 straw burning points in the province were monitored by satellite remote sensing from January to October 2022. The proportion of industrial emission and solvent use decreased during the pollution periods, indicating that the implementation of shutdown or off-peak production measures at the time of pollution warning were effective.

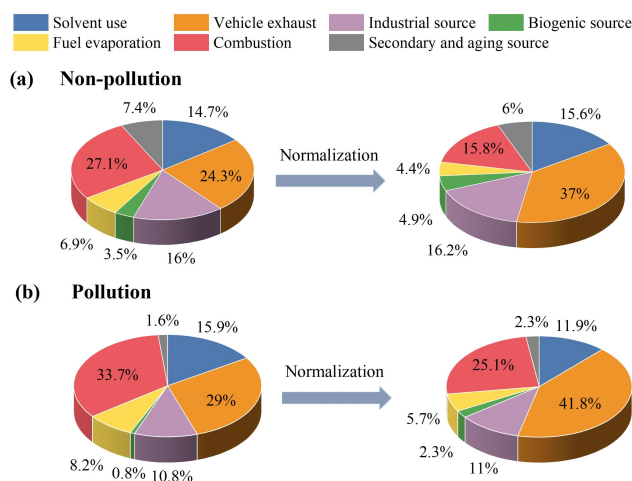


Figure 8: Comparison of VOCs sources proportion before and after meteorological normalization during the non-pollution periods and pollution periods in the warm season in 2022.

425

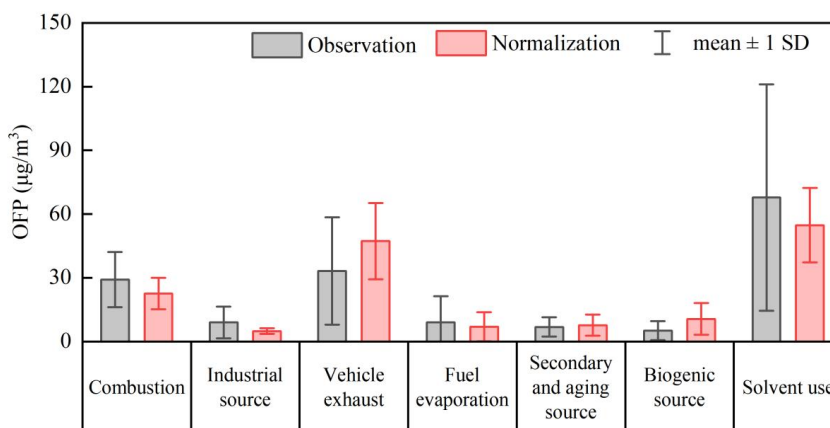
The O₃ formation potential (OFP) is used to assess VOC photochemical activity (Carter, 2010), and it can be calculated by using Eq. (2):

$$OFP_i = MIR_i \times [VOC_i] \quad (2)$$

Where MIR_i represents the maximum incremental reactivity for VOC species i . $[VOC_i]$ represents the concentration of VOC species i ($\mu\text{g}/\text{m}^3$). MIR value for each VOC species were taken from the updated Carter research results (<http://www.engr.ucr.edu/~carter/reactdat.htm>, last access: 24 February 2021). The contributions of emission sources to OFP was further analyzed and shown in Fig. 9. Based on the result of the observation, the emission sources that contribute the most to OFP were solvent use (67.79



$\mu\text{g}/\text{m}^3$), vehicle exhaust ($33.16 \mu\text{g}/\text{m}^3$) and combustion ($29.16 \mu\text{g}/\text{m}^3$) during the pollution periods in
 435 the warm season in 2022. After removing the effect of dispersion, the contribution of vehicle exhaust to
 OPF increased to $47.25 \mu\text{g}/\text{m}^3$, while the contribution of solvent use and combustion to OPF decreased
 to $54.77 \mu\text{g}/\text{m}^3$ and $22.58 \mu\text{g}/\text{m}^3$, respectively. The actual contributions of combustion and solvent use
 to O_3 formation were larger under dispersion effect. Thus, it was necessary to consider the cumulative
 effect of dispersion and enhance emission reduction measures for specific emission sources. For the
 440 Period 2 mentioned in section 3.1.3, we also found that the contributions of VOCs emission sources
 changed after meteorological normalization (Fig. S5 and Fig .S6). After removing the dispersion effect,
 the contributions of solvent use and vehicle exhaust to OPF increased during the pollution, while the
 contribution of combustion and secondary and aging source decreased. From August 17 to August 19,
 the normalized contribution of solvent source to OPF was significant, with an average OPF of 105.81
 445 $\mu\text{g}/\text{m}^3$, indicating that the emission of solvent source was enhanced in these days. The dispersion effect
 of meteorological conditions on precursors can conceal the real information of emission sources and
 misjudge the formation process of O_3 .



450 **Figure 9: The contributions of emission sources to OPF based on observation and meteorological normalization during the pollution periods in the warm season in 2022.**



4 Conclusion

In this paper, a RF model was established based on the hourly data of four years of continuous
455 observation, and some meteorological effects on the concentration time series of air pollutants were
removed. Transport and dispersion effects were removed for O₃ and dispersion effect was removed for
its precursors. In the process of building the RF model, UVB, RH and T were found to be the most
important factors affecting O₃ concentration, with the importance of 25.9%, 18.2% and 11.3%,
respectively. Local influences, including precursor emissions and secondary photochemical reactions,
460 occupied 83.9% of the importance to O₃ concentration. To understand the mechanisms of local O₃
formation, the meteorological effects were analyzed in long-term trends, pollution and non-pollution
periods in the warm season, as well as short-term pollution events. After decoupling meteorological
effects, the concentration trends of O₃ was consistent with those observed in the long term, indicating
that O₃ concentration was mainly driven by precursor emissions and local chemical reactions. During
465 the pollution periods in the warm season from 2019 to 2022, the positive contributions of dispersion
and transport to the MDA8 O₃ ranged from 12.9% to 24.0%. The effects of dispersion and transport
were further analyzed for different types of O₃ pollution events. For transmission-type O₃ pollution
(Period 1), dispersion and transport contributed 18.7% to the MDA8 O₃ concentration, increasing the
mean MDA8 O₃ concentration from 157 µg/m³ to 193 µg/m³. For local and transmission-type O₃
470 pollution (Period 2), the average locally generated MDA8 O₃ concentration was 185 µg/m³. Under the
influences of dispersion and transport, the average MDA8 O₃ concentration increased to 211 µg/m³,
and the positive contributions of dispersion and transport ranged from 8.5% to 20.4%. BLH, as a
parameter of dispersion, was of the highest importance for NO₂ and NMHCs, accounting for 34.2% to
NO₂ and 30.7% to NMHCs. Therefore, precursor concentrations were accumulated even in the case of
475 low emissions when the dispersion condition was poor, promoting the photochemical production of O₃.
This also corresponds to the fact that even with the implementation of precursor emission reduction
policies, O₃ concentrations in urban areas remain persistently high.

By decoupling the influences of meteorological conditions, it was observed that the sensitivity of local
O₃ formation and the apportionment of VOCs emission sources have changed. From the EKMA of
480 short-term pollution event, the sensitivity of O₃ formation in Period 2 changed from the NO_x-limited
regime to the transition regime between VOC- and NO_x-limited regimes after meteorological



normalization. Based on PMF model, the changes of VOCs emission sources after the removal of dispersion effect during the warm season in 2022 were further analyzed. After removing the effect of dispersion, the absolute contribution of vehicle exhaust to VOCs during the pollution was 9.76 ppbv, 485 accounting for 41.8%, and the contribution of vehicle exhaust to OFP was 47.25 $\mu\text{g}/\text{m}^3$. The contribution of vehicle exhaust to VOCs was underestimated due the dispersion effect. After meteorological normalization, combustion remained an important source of VOCs, contributing 25.1% during the pollution period, which was overestimated by 8.6%. The normalized contribution of solvent use to VOCs decreased to 11.9%, but it is undeniable that solvent use was still a crucial contributor to 490 OFP, contributing 54.77 $\mu\text{g}/\text{m}^3$. Neglecting the influences of meteorology can lead to a deviation in emission reduction priorities, and the effectiveness of emission reduction may be masked by unfavorable meteorological conditions. The conclusion of this research suggested that meteorological fluctuations can interfere with the results of OBM and PMF. Decoupling meteorological effects before using traditional models was beneficial for deepening the understanding of local O_3 formation and 495 improving the rationality of precursor emission reduction measures.



Data availability. The data used in this study are available upon request from Yuqing Qiu (yuqing.qiu@stu.pku.edu.cn) and Xin Li (li_xin@pku.edu.cn).

Author contributions. XL, WC, and YZ conceived and designed this study, and revised the Article critically. YQ and XL analysed and interpreted data, drafted the Article, and revised it critically. YL and MS contributed to the modeling of the data. XT, QZ, WL, WZ, and JL acquired the field observation data.

Competing interests. The authors declare that they have no conflict of interest.

Acknowledgements. The authors are grateful to the Zhejiang Ecological and Environmental Monitoring Center and Jinhua Ecological and Environmental Monitoring Center for observation in this study. This work was supported by the Beijing Municipal Natural Science Fund (JQ21030) and by the National Key R&D Program of China (2022YFC3700302).

Financial support. This research has been supported by the Beijing Municipal Natural Science Fund (JQ21030) and the National Key R&D Program of China (2022YFC3700302).



510 **References**

- Ahmad, W., Coeur, C., Tomas, A., Fagniez, T., Brubach, J.-B., and Cuisset, A.: Infrared spectroscopy of secondary organic aerosol precursors and investigation of the hygroscopicity of SOA formed from the OH reaction with guaiacol and syringol, *Appl. Opt.*, 56, E116-E122, <https://doi.org/10.1364/ao.56.00e116>, 2017.
- 515 Atkinson, R.: Atmospheric chemistry of VOCs and NO_x, *Atmos. Environ.*, 34, 2063-2101, [https://doi.org/10.1016/s1352-2310\(99\)00460-4](https://doi.org/10.1016/s1352-2310(99)00460-4), 2000.
- Borbon, A., Gilman, J. B., Kuster, W. C., Grand, N., Chevaillier, S., Colomb, A., Dolgorouky, C., Gros, V., Lopez, M., Sarda-Esteve, R., Holloway, J., Stutz, J., Petetin, H., McKeen, S., Beekmann, M., Warneke, C., Parrish, D. D., and de Gouw, J. A.: Emission ratios of anthropogenic volatile organic
- 520 compounds in northern mid-latitude megacities: Observations versus emission inventories in Los Angeles and Paris, *J. Geophys. Res.-Atmos.*, 118, 2041-2057, <https://doi.org/10.1002/jgrd.50059>, 2013.
- Cai, C., Geng, F., Tie, X., Yu, Q., and An, J.: Characteristics and source apportionment of VOCs measured in Shanghai, China, *Atmos. Environ.*, 44, 5005-5014, <https://doi.org/10.1016/j.atmosenv.2010.07.059>, 2010.
- 525 Carslaw, D. C. and Taylor, P. J.: Analysis of air pollution data at a mixed source location using boosted regression trees, *Atmos. Environ.*, 43, 3563-3570, <https://doi.org/10.1016/j.atmosenv.2009.04.001>, 2009.
- Carter, W. P. L.: Development of the SAPRC-07 chemical mechanism, *Atmos. Environ.*, 44, 5324-5335, <https://doi.org/10.1016/j.atmosenv.2010.01.026>, 2010.
- 530 Chinese State Council: Action Plan on Air Pollution Prevention and Control (in Chinese), available at: https://www.gov.cn/gongbao/content/2013/content_2496394.htm (last access: 28 March 2024), 2013.
- Chinese State Council: Three-Year Action Plan on Defending the Blue Sky (in Chinese), available at: http://www.gov.cn/zhengce/content/2018-07/03/content_5303158.htm (last access: 28 March 2024), 2018.
- 535 Cohen, A. J., Brauer, M., Burnett, R., Anderson, H. R., Frostad, J., Estep, K., Balakrishnan, K., Brunekreef, B., Dandona, L., Dandona, R., Feigin, V., Freedman, G., Hubbell, B., Jobling, A., Kan, H., Knibbs, L., Liu, Y., Martin, R., Morawska, L., Pope, C. A., III, Shin, H., Straif, K., Shaddick, G., Thomas, M., van Dingenen, R., van Donkelaar, A., Vos, T., Murray, C. J. L., and Forouzanfar, M. H.:



- Estimates and 25-year trends of the global burden of disease attributable to ambient air pollution: an
540 analysis of data from the Global Burden of Diseases Study 2015, *Lancet*, 389, 1907-1918,
[https://doi.org/10.1016/s0140-6736\(17\)30505-6](https://doi.org/10.1016/s0140-6736(17)30505-6), 2017.
- Cui, L. and Wang, S.: Mapping the daily nitrous acid (HONO) concentrations across China during 2006
–2017 through ensemble machine-learning algorithm, *Sci. Total Environ.*, 785,
<https://doi.org/10.1016/j.scitotenv.2021.147325>, 2021.
- 545 Dai, Q., Liu, B., Bi, X., Wu, J., Liang, D., Zhang, Y., Feng, Y., and Hopke, P. K.: Dispersion
Normalized PMF Provides Insights into the Significant Changes in Source Contributions to PM_{2.5} after
the COVID-19 Outbreak, *Environ. Sci. Technol.*, 54, 9917-9927,
<https://doi.org/10.1021/acs.est.0c02776>, 2020.
- Dai, T., Dai, Q., Ding, J., Liu, B., Bi, X., Wu, J., Zhang, Y., and Feng, Y.: Measuring the Emission
550 Changes and Meteorological Dependence of Source-Specific BC Aerosol Using Factor Analysis
Coupled With Machine Learning, *J. Geophys. Res.-Atmos.*, 128,
<https://doi.org/10.1029/2023jd038696>, 2023.
- Dang, R., Liao, H., and Fu, Y.: Quantifying the anthropogenic and meteorological influences on
summertime surface ozone in China over 2012-2017, *Sci. Total Environ.*, 754,
555 <https://doi.org/10.1016/j.scitotenv.2020.142394>, 2021.
- de Gouw, J. A., Warneke, C., Parrish, D. D., Holloway, J. S., Trainer, M., and Fehsenfeld, F. C.:
Emission sources and ocean uptake of acetonitrile (CH₃CN) in the atmosphere, *J. Geophys. Res.-
Atmos.*, 108, <https://doi.org/10.1029/2002jd002897>, 2003.
- Ding, J., Dai, Q., Fan, W., Lu, M., Zhang, Y., Han, S., and Feng, Y.: Impacts of meteorology and
560 precursor emission change on O₃ variation in Tianjin, China from 2015 to 2021, *J. Environ. Sci.*, 126,
506-516, <https://doi.org/10.1016/j.jes.2022.03.010>, 2023.
- Feng, R., Zheng, H.-j., Zhang, A.-r., Huang, C., Gao, H., and Ma, Y.-c.: Unveiling tropospheric ozone
by the traditional atmospheric model and machine learning, and their comparison: A case study in
hangzhou, China, *Environ. Pollut.*, 252, 366-378, <https://doi.org/10.1016/j.envpol.2019.05.101>,
565 2019.
- Fu, Y., Liao, H., and Yang, Y.: Interannual and Decadal Changes in Tropospheric Ozone in China and
the Associated Chemistry-Climate Interactions: A Review, *Adv. Atmos. Sci.*, 36, 975-993,
<https://doi.org/10.1007/s00376-019-8216-9>, 2019.



- Gao, D., Xie, M., Liu, J., Wang, T., Ma, C., Bai, H., Chen, X., Li, M., Zhuang, B., and Li, S.: Ozone
570 variability induced by synoptic weather patterns in warm seasons of 2014–2018 over the Yangtze River
Delta region, China, *Atmos. Chem. Phys.*, 21, 5847-5864, <https://doi.org/10.5194/acp-21-5847-2021>,
2021.
- Goliff, W. S., Stockwell, W. R., and Lawson, C. V.: The regional atmospheric chemistry mechanism,
version 2, *Atmos. Environ.*, 68, 174-185, <https://doi.org/10.1016/j.atmosenv.2012.11.038>, 2013.
- 575 Gong, D., Wang, H., Zhang, S., Wang, Y., Liu, S. C., Guo, H., Shao, M., He, C., Chen, D., He, L.,
Zhou, L., Morawska, L., Zhang, Y., and Wang, B.: Low-level summertime isoprene observed at a
forested mountaintop site in southern China: implications for strong regional atmospheric oxidative
capacity, *Atmos. Chem. Phys.*, 18, 14417-14432, <https://doi.org/10.5194/acp-18-14417-2018>, 2018.
- Grange, S. K. and Carslaw, D. C.: Using meteorological normalisation to detect interventions in air
580 quality time series, *Sci. Total Environ.*, 653, 578-588, <https://doi.org/10.1016/j.scitotenv.2018.10.344>,
2019.
- Grange, S. K., Carslaw, D. C., Lewis, A. C., Boleti, E., and Hueglin, C.: Random forest meteorological
normalisation models for Swiss PM₁₀ trend analysis, *Atmos. Chem. Phys.*, 18, 6223-6239,
<https://doi.org/10.5194/acp-18-6223-2018>, 2018.
- 585 Guo, Y., Li, K., Zhao, B., Shen, J., Bloss, W. J., Azzi, M., and Zhang, Y.: Evaluating the real changes of
air quality due to clean air actions using a machine learning technique: Results from 12 Chinese mega-
cities during 2013–2020, *Chemosphere*, 300, <https://doi.org/10.1016/j.chemosphere.2022.134608>,
2022.
- Han, H., Liu, J., Shu, L., Wang, T., and Yuan, H.: Local and synoptic meteorological influences on
590 daily variability in summertime surface ozone in eastern China, *Atmos. Chem. Phys.*, 20, 203-222,
<https://doi.org/10.5194/acp-20-203-2020>, 2020.
- Han, H., Liu, J., Yuan, H., Wang, T., Zhuang, B., and Zhang, X.: Foreign influences on tropospheric
ozone over East Asia through global atmospheric transport, *Atmos. Chem. Phys.*, 19, 12495-12514,
<https://doi.org/10.5194/acp-19-12495-2019>, 2019.
- 595 Hersbach, H., Bell, B., Berrisford, P., Hirahara, S., Horányi, A., Muñoz-Sabater, J., Nicolas, J., Peubey,
C., Radu, R., Schepers, D., Simmons, A., Soci, C., Abdalla, S., Abellan, X., Balsamo, G., Bechtold, P.,
Biavati, G., Bidlot, J., Bonavita, M., De Chiara, G., Dahlgren, P., Dee, D., Diamantakis, M., Dragani,
R., Flemming, J., Forbes, R., Fuentes, M., Geer, A., Haimberger, L., Healy, S., Hogan, R. J., Hólm, E.,



- Janisková, M., Keeley, S., Laloyaux, P., Lopez, P., Lupu, C., Radnoti, G., de Rosnay, P., Rozum, I.,
600 Vamborg, F., Villaume, S., and Thépaut, J.-N.: The ERA5 global reanalysis, *Q. J. Roy. Meteor. Soc.*,
146, 1999–2049, <https://doi.org/10.1002/qj.3803>, 2020.
- Hou, L., Dai, Q., Song, C., Liu, B., Guo, F., Dai, T., Li, L., Liu, B., Bi, X., Zhang, Y., and Feng, Y.:
Revealing Drivers of Haze Pollution by Explainable Machine Learning, *Environ. Sci. Technol. Lett.*, 9,
112-119, <https://doi.org/10.1021/acs.estlett.1c00865>, 2022.
- 605 Hu, C., Kang, P., Jaffé, D. A., Li, C., Zhang, X., Wu, K., and Zhou, M.: Understanding the impact of
meteorology on ozone in 334 cities of China, *Atmos. Environ.*, 248,
<https://doi.org/10.1016/j.atmosenv.2021.118221>, 2021.
- Huang, X., Huang, J., Ren, C., Wang, J., Wang, H., Wang, J., Yu, H., Chen, J., Gao, J., and Ding, A.:
Chemical Boundary Layer and Its Impact on Air Pollution in Northern China, *Environ. Sci. Technol.*
610 *Let.*, 7, 826-832, <https://doi.org/10.1021/acs.estlett.0c00755>, 2020.
- Kong, L., Song, M., Li, X., Liu, Y., Lu, S., Zeng, L., and Zhang, Y.: Analysis of China's PM_{2.5} and
ozone coordinated control strategy based on the observation data from 2015 to 2020, *J. Environ. Sci.*,
138, 385-394, <https://doi.org/10.1016/j.jes.2023.03.030>, 2024.
- Lei, Y., Wu, K., Zhang, X., Kang, P., Du, Y., Yang, F., Fan, J., and Hou, J.: Role of meteorology-driven
615 regional transport on O₃ pollution over the Chengdu Plain, southwestern China, *Atmos. Res.*, 285,
<https://doi.org/10.1016/j.atmosres.2023.106619>, 2023.
- Li, C., Zhu, Q., Jin, X., and Cohen, R. C.: Elucidating Contributions of Anthropogenic Volatile Organic
Compounds and Particulate Matter to Ozone Trends over China, *Environ. Sci. Technol.*, 56, 12906-
12916, <https://doi.org/10.1021/acs.est.2c03315>, 2022a.
- 620 Li, K., Jacob, D. J., Shen, L., Lu, X., De Smedt, I., and Liao, H.: Increases in surface ozone pollution in
China from 2013 to 2019: anthropogenic and meteorological influences, *Atmos. Chem. Phys.*, 20,
11423-11433, <https://doi.org/10.5194/acp-20-11423-2020>, 2020.
- Li, L., Xie, F., Li, J., Gong, K., Xie, X., Qin, Y., Qin, M., and Hu, J.: Diagnostic analysis of regional
ozone pollution in Yangtze River Delta, China: A case study in summer 2020, *Sci. Total Environ.*, 812,
625 <https://doi.org/10.1016/j.scitotenv.2021.151511>, 2022b.
- Li, L., Chen, C. H., Huang, C., Huang, H. Y., Zhang, G. F., Wang, Y. J., Wang, H. L., Lou, S. R., Qiao,
L. P., Zhou, M., Chen, M. H., Chen, Y. R., Streets, D. G., Fu, J. S., and Jang, C. J.: Process analysis of
regional ozone formation over the Yangtze River Delta, China using the Community Multi-scale Air



Quality modeling system, *Atmos. Chem. Phys.*, 12, 10971-10987, <https://doi.org/10.5194/acp-12-10971-2012>, 2012.

Liu, B., Wang, Y., Meng, H., Dai, Q., Diao, L., Wu, J., Shi, L., Wang, J., Zhang, Y., and Feng, Y.: Dramatic changes in atmospheric pollution source contributions for a coastal megacity in northern China from 2011 to 2020, *Atmos. Chem. Phys.*, 22, 8597-8615, <https://doi.org/10.5194/acp-22-8597-2022>, 2022a.

Liu, H., Yue, F., and Xie, Z.: Quantify the role of anthropogenic emission and meteorology on air pollution using machine learning approach: A case study of PM_{2.5} during the COVID-19 outbreak in Hubei Province, China, *Environ. Pollut.*, 300, <https://doi.org/10.1016/j.envpol.2022.118932>, 2022b.

Liu, X., Lu, D., Zhang, A., Liu, Q., and Jiang, G.: Data-Driven Machine Learning in Environmental Pollution: Gains and Problems, *Environ. Sci. Technol.*, 56, 2124-2133, <https://doi.org/10.1021/acs.est.1c06157>, 2022c.

Liu, Y. and Wang, T.: Worsening urban ozone pollution in China from 2013 to 2017-Part 1: The complex and varying roles of meteorology, *Atmos. Chem. Phys.*, 20, 6305-6321, <https://doi.org/10.5194/acp-20-6305-2020>, 2020.

Liu, Y., Shao, M., Fu, L., Lu, S., Zeng, L., and Tang, D.: Source profiles of volatile organic compounds (VOCs) measured in China: Part I, *Atmos. Environ.*, 42, 6247-6260, <https://doi.org/10.1016/j.atmosenv.2008.01.070>, 2008.

Liu, Y., Geng, G., Cheng, J., Liu, Y., Xiao, Q., Liu, L., Shi, Q., Tong, D., He, K., and Zhang, Q.: Drivers of Increasing Ozone during the Two Phases of Clean Air Actions in China 2013–2020, *Environ. Sci. Technol.*, 57, 8954-8964, <https://doi.org/10.1021/acs.est.3c00054>, 2023.

Lu, X., Zhang, L., and Shen, L.: Meteorology and Climate Influences on Tropospheric Ozone: a Review of Natural Sources, Chemistry, and Transport Patterns, *Curr. Pollut. Rep.*, 5, 238-260, <https://doi.org/10.1007/s40726-019-00118-3>, 2019.

Lumiaro, E., Todorović, M., Kurten, T., Vehkamäki, H., and Rinke, P.: Predicting gas–particle partitioning coefficients of atmospheric molecules with machine learning, *Atmos. Chem. Phys.*, 21, 13227-13246, <https://doi.org/10.5194/acp-21-13227-2021>, 2021.

Lv, Y., Tian, H., Luo, L., Liu, S., Bai, X., Zhao, H., Zhang, K., Lin, S., Zhao, S., Guo, Z., Xiao, Y., and Yang, J.: Understanding and revealing the intrinsic impacts of the COVID-19 lockdown on air quality



- and public health in North China using machine learning, *Sci. Total Environ.*, 857, <https://doi.org/10.1016/j.scitotenv.2022.159339>, 2023.
- 660 Ma, L., Graham, D. J., and Stettler, M. E. J.: Using Explainable Machine Learning to Interpret the Effects of Policies on Air Pollution: COVID-19 Lockdown in London, *Environ. Sci. Technol.*, 57, 18271-18281, <https://doi.org/10.1021/acs.est.2c09596>, 2023.
- Ma, X., Huang, J., Zhao, T., Liu, C., Zhao, K., Xing, J., and Xiao, W.: Rapid increase in summer surface ozone over the North China Plain during 2013–2019: a side effect of particulate matter reduction control?, *Atmos. Chem. Phys.*, 21, 1-16, <https://doi.org/10.5194/acp-21-1-2021>, 2021.
- 665 Miller, S. L., Anderson, M. J., Daly, E. P., and Milford, J. B.: Source apportionment of exposures to volatile organic compounds. I. Evaluation of receptor models using simulated exposure data, *Atmos. Environ.*, 36, 3629-3641, [https://doi.org/10.1016/s1352-2310\(02\)00279-0](https://doi.org/10.1016/s1352-2310(02)00279-0), 2002.
- Ministry of Ecology and Environment (MEE): Revision of the Ambient air quality standards (GB 3095-2012) (in Chinese), available at: https://www.mee.gov.cn/xxgk/xxgk01/201808/t20180815_629602.html (last access: 28 March 2022), 2018.
- Mo, Z., Shao, M., Wang, W., Liu, Y., Wang, M., and Lu, S.: Evaluation of biogenic isoprene emissions and their contribution to ozone formation by ground-based measurements in Beijing, China, *Sci. Total Environ.*, 627, 1485-1494, <https://doi.org/10.1016/j.scitotenv.2018.01.336>, 2018.
- 675 Monks, P. S., Archibald, A. T., Colette, A., Cooper, O., Coyle, M., Derwent, R., Fowler, D., Granier, C., Law, K. S., Mills, G. E., Stevenson, D. S., Tarasova, O., Thouret, V., von Schneidmesser, E., Sommariva, R., Wild, O., and Williams, M. L.: Tropospheric ozone and its precursors from the urban to the global scale from air quality to short-lived climate forcer, *Atmos. Chem. Phys.*, 15, 8889-8973, <https://doi.org/10.5194/acp-15-8889-2015>, 2015.
- 680 Mousavinezhad, S., Choi, Y., Pouyaei, A., Ghahremanloo, M., and Nelson, D. L.: A comprehensive investigation of surface ozone pollution in China, 2015-2019: Separating the contributions from meteorology and precursor emissions, *Atmos. Res.*, 257, <https://doi.org/10.1016/j.atmosres.2021.105599>, 2021.
- 685 Paatero, P. and Tapper, U.: Positive matrix factorization: A non-negative factor model with optimal utilization of error estimates of data values, *Environmetrics*, 5, 111-126, <https://doi.org/10.1002/env.3170050203>, 1994.



- Peng, X., Xie, T.-T., Tang, M.-X., Cheng, Y., Peng, Y., Wei, F.-H., Cao, L.-M., Yu, K., Du, K., He, L.-Y., and Huang, X.-F.: Critical Role of Secondary Organic Aerosol in Urban Atmospheric Visibility Improvement Identified by Machine Learning, *Environ. Sci. Technol. Lett.*, 10, 976-982, <https://doi.org/10.1021/acs.estlett.3c00084>, 2023.
- Song, C., Liu, B., Cheng, K., Cole, M. A., Dai, Q., Elliott, R. J. R., and Shi, Z.: Attribution of Air Quality Benefits to Clean Winter Heating Policies in China: Combining Machine Learning with Causal Inference, *Environ. Sci. Technol.*, 57, 17707-17717, <https://doi.org/10.1021/acs.est.2c06800>, 2023.
- 690 Song, M., Tan, Q., Feng, M., Qu, Y., Liu, X., An, J., and Zhang, Y.: Source Apportionment and Secondary Transformation of Atmospheric Nonmethane Hydrocarbons in Chengdu, Southwest China, *J. Geophys. Res.-Atmos.*, 123, 9741-9763, <https://doi.org/10.1029/2018jd028479>, 2018.
- Song, M., Li, X., Yang, S., Yu, X., Zhou, S., Yang, Y., Chen, S., Dong, H., Liao, K., Chen, Q., Lu, K., Zhang, N., Cao, J., Zeng, L., and Zhang, Y.: Spatiotemporal variation, sources, and secondary transformation potential of volatile organic compounds in Xi'an, China, *Atmos. Chem. Phys.*, 21, 4939-4958, <https://doi.org/10.5194/acp-21-4939-2021>, 2021a.
- 700 Song, Z., Bai, Y., Wang, D., Li, T., and He, X.: Satellite Retrieval of Air Pollution Changes in Central and Eastern China during COVID-19 Lockdown Based on a Machine Learning Model, *Remote Sens.*, 13, <https://doi.org/10.3390/rs13132525>, 2021b.
- 705 Stein, A. F., Draxler, R. R., Rolph, G. D., Stunder, B. J. B., Cohen, M. D., and Ngan, F.: NOAA's HYSPLIT Atmospheric Transport and Dispersion Modeling System, *Bull. Am. Meteorol. Soc.*, 96, 2059-2077, <https://doi.org/10.1175/bams-d-14-00110.1>, 2015.
- Sun, J., Wu, F., Hu, B., Tang, G., Zhang, J., and Wang, Y.: VOC characteristics, emissions and contributions to SOA formation during hazy episodes, *Atmos. Environ.*, 141, 560-570, <https://doi.org/10.1016/j.atmosenv.2016.06.060>, 2016.
- 710 Tan, Z., Lu, K., Jiang, M., Su, R., Dong, H., Zeng, L., Xie, S., Tan, Q., and Zhang, Y.: Exploring ozone pollution in Chengdu, southwestern China: A case study from radical chemistry to O₃-VOC-NO_x sensitivity, *Sci. Total Environ.*, 636, 775-786, <https://doi.org/10.1016/j.scitotenv.2018.04.286>, 2018.
- Tan, Z., Fuchs, H., Lu, K., Hofzumahaus, A., Bohn, B., Broch, S., Dong, H., Gomm, S., Häseler, R., He, L., Holland, F., Li, X., Liu, Y., Lu, S., Rohrer, F., Shao, M., Wang, B., Wang, M., Wu, Y., Zeng, L., Zhang, Y., Wahner, A., and Zhang, Y.: Radical chemistry at a rural site (Wangdu) in the North China



- Plain: observation and model calculations of OH, HO₂ and RO₂ radicals, *Atmos. Chem. Phys.*, 17, 663-690, <https://doi.org/10.5194/acp-17-663-2017>, 2017.
- 720 Tang, J.-H., Pan, S.-R., Li, L., and Chan, P.-W.: A machine learning-based method for identifying the meteorological field potentially inducing ozone pollution, *Atmos. Environ.*, 312, <https://doi.org/10.1016/j.atmosenv.2023.120047>, 2023.
- Tesch, T., Kollet, S., and Garcke, J.: Causal deep learning models for studying the Earth system, *Geoscientific Model Development*, 16, 2149-2166, <https://doi.org/10.5194/gmd-16-2149-2023>, 2023.
- 725 Vu, T. V., Shi, Z., Cheng, J., Zhang, Q., He, K., Wang, S., and Harrison, R. M.: Assessing the impact of clean air action on air quality trends in Beijing using a machine learning technique, *Atmos. Chem. Phys.*, 19, 11303-11314, <https://doi.org/10.5194/acp-19-11303-2019>, 2019.
- Wang, M., Shao, M., Chen, W., Lu, S., Liu, Y., Yuan, B., Zhang, Q., Zhang, Q., Chang, C. C., Wang, B., Zeng, L., Hu, M., Yang, Y., and Li, Y.: Trends of non-methane hydrocarbons (NMHC) emissions in Beijing during 2002–2013, *Atmos. Chem. Phys.*, 15, 1489-1502, [https://doi.org/10.5194/acp-15-1489-](https://doi.org/10.5194/acp-15-1489-2015)
730 2015, 2015.
- Wang, Y., Shen, L., Wu, S., Mickley, L., He, J., and Hao, J.: Sensitivity of surface ozone over China to 2000-2050 global changes of climate and emissions, *Atmos. Environ.*, 75, 374-382, <https://doi.org/10.1016/j.atmosenv.2013.04.045>, 2013.
- 735 Wang, Y., Jiang, S., Huang, L., Lu, G., Kasemsan, M., Yaluk, E. A., Liu, H., Liao, J., Bian, J., Zhang, K., Chen, H., and Li, L.: Differences between VOCs and NO_x transport contributions, their impacts on O₃, and implications for O₃ pollution mitigation based on CMAQ simulation over the Yangtze River Delta, China, *Sci. Total Environ.*, 872, <https://doi.org/10.1016/j.scitotenv.2023.162118>, 2023.
- Wei, J., Li, Z., Wang, J., Li, C., Gupta, P., and Cribb, M.: Ground-level gaseous pollutants (NO₂, SO₂, and CO) in China: daily seamless mapping and spatiotemporal variations, *Atmos. Chem. Phys.*, 23, 1511-1532, <https://doi.org/10.5194/acp-23-1511-2023>, 2023.
- 740 Weng, X., Forster, G. L., and Nowack, P.: A machine learning approach to quantify meteorological drivers of ozone pollution in China from 2015 to 2019, *Atmos. Chem. Phys.*, 22, 8385-8402, <https://doi.org/10.5194/acp-22-8385-2022>, 2022.
- Wolfe, G. M., Kaiser, J., Hanisco, T. F., Keutsch, F. N., de Gouw, J. A., Gilman, J. B., Graus, M., Hatch, C. D., Holloway, J., Horowitz, L. W., Lee, B. H., Lerner, B. M., Lopez-Hilifiker, F., Mao, J., Marvin, M. R., Peischl, J., Pollack, I. B., Roberts, J. M., Ryerson, T. B., Thornton, J. A., Veres, P. R.,



- and Warneke, C.: Formaldehyde production from isoprene oxidation across NO_x regimes, *Atmos. Chem. Phys.*, 16, 2597-2610, <https://doi.org/10.5194/acp-16-2597-2016>, 2016.
- Wu, Y., Liu, B., Meng, H., Dai, Q., Shi, L., Song, S., Feng, Y., and Hopke, P. K.: Changes in source
750 apportioned VOCs during high O₃ periods using initial VOC-concentration-dispersion normalized
PMF, *Sci. Total Environ.*, 896, <https://doi.org/10.1016/j.scitotenv.2023.165182>, 2023.
- Yang, C., Dong, H., Chen, Y., Wang, Y., Fan, X., Tham, Y. J., Chen, G., Xu, L., Lin, Z., Li, M., Hong,
Y., and Chen, J.: Machine Learning Reveals the Parameters Affecting the Gaseous Sulfuric Acid
Distribution in a Coastal City: Model Construction and Interpretation, *Environ. Sci. Technol. Lett.*, 10,
755 1045-1051, <https://doi.org/10.1021/acs.estlett.3c00170>, 2023.
- Yang, J., Wen, Y., Wang, Y., Zhang, S., Pinto, J. P., Pennington, E. A., Wang, Z., Wu, Y., Sander, S. P.,
Jiang, J. H., Hao, J., Yung, Y. L., and Seinfeld, J. H.: From COVID-19 to future electrification:
Assessing traffic impacts on air quality by a machine-learning model, *P. Natl. Acad. Sci. USA*, 118,
<https://doi.org/10.1073/pnas.2102705118>, 2021a.
- 760 Yang, L., Luo, H., Yuan, Z., Zheng, J., Huang, Z., Li, C., Lin, X., Louie, P. K. K., Chen, D., and Bian,
Y.: Quantitative impacts of meteorology and precursor emission changes on the long-term trend of
ambient ozone over the Pearl River Delta, China, and implications for ozone control strategy, *Atmos.
Chem. Phys.*, 19, 12901-12916, <https://doi.org/10.5194/acp-19-12901-2019>, 2019.
- Yang, S., Li, X., Song, M., Liu, Y., Yu, X., Chen, S., Lu, S., Wang, W., Yang, Y., Zeng, L., and Zhang,
765 Y.: Characteristics and sources of volatile organic compounds during pollution episodes and clean
periods in the Beijing-Tianjin-Hebei region, *Sci. Total Environ.*, 799,
<https://doi.org/10.1016/j.scitotenv.2021.149491>, 2021b.
- Ye, X., Wang, X., and Zhang, L.: Diagnosing the Model Bias in Simulating Daily Surface Ozone
Variability Using a Machine Learning Method: The Effects of Dry Deposition and Cloud Optical
770 Depth, *Environ. Sci. Technol.*, 56, 16665-16675, <https://doi.org/10.1021/acs.est.2c05712>, 2022.
- Yuan, B., Shao, M., Lu, S., and Wang, B.: Source profiles of volatile organic compounds associated
with solvent use in Beijing, China, *Atmos. Environ.*, 44, 1919-1926,
<https://doi.org/10.1016/j.atmosenv.2010.02.014>, 2010.
- Zhang, H., Wang, Y., Hu, J., Ying, Q., and Hu, X.-M.: Relationships between meteorological
775 parameters and criteria air pollutants in three megacities in China, *Environ. Res.*, 140, 242-254,
<https://doi.org/10.1016/j.envres.2015.04.004>, 2015.



- Zhang, K., Liu, Z., Zhang, X., Li, Q., Jensen, A., Tan, W., Huang, L., Wang, Y., de Gouw, J., and Li, L.: Insights into the significant increase in ozone during COVID-19 in a typical urban city of China, *Atmos. Chem. Phys.*, 22, 4853-4866, <https://doi.org/10.5194/acp-22-4853-2022>, 2022.
- 780 Zhang, L., Wang, L., Ji, D., Xia, Z., Nan, P., Zhang, J., Li, K., Qi, B., Du, R., Sun, Y., Wang, Y., and Hu, B.: Explainable ensemble machine learning revealing the effect of meteorology and sources on ozone formation in megacity Hangzhou, China, *Sci. Total Environ.*, 922, <https://doi.org/10.1016/j.scitotenv.2024.171295>, 2024.
- Zhang, Q., He, K., and Huo, H.: Cleaning China's air, *Nature*, 484, 161-162, 10.1038/484161a, 2012.
- 785 Zheng, B., Tong, D., Li, M., Liu, F., Hong, C., Geng, G., Li, H., Li, X., Peng, L., Qi, J., Yan, L., Zhang, Y., Zhao, H., Zheng, Y., He, K., and Zhang, Q.: Trends in China's anthropogenic emissions since 2010 as the consequence of clean air actions, *Atmos. Chem. Phys.*, 18, 14095-14111, <https://doi.org/10.5194/acp-18-14095-2018>, 2018.
- Zhu, Q., Laughner, J. L., and Cohen, R. C.: Estimate of OH trends over one decade in North American
790 cities, *P. Natl. Acad. Sci. USA*, 119, <https://doi.org/10.1073/pnas.2117399119>, 2022.